Available online at www.sciencedirect.com
ScienceDirect
Surface Science 600 (2006) 3327–3336
SURFACE SCIENCE
www.elsevier.com/locate/susc

Initial growth of platinum on oxygen-covered Ni(1 1 0) surfaces

M. Walker, C.R. Parkinson [1], M. Draxler [2], M.G. Brown, C.F. McConville *

Department of Physics, University of Warwick, Coventry CV4 7AL, United Kingdom

Received 22 May 2006; accepted for publication 20 June 2006
Available online 17 July 2006

Abstract

The initial growth of Pt on the Ni(1 1 0)–(3 × 1)-O and NiO(1 1 0) surfaces has been studied by coaxial impact collision ion scattering spectroscopy (CAICISS), low energy electron diffraction (LEED) and X-ray photoelectron spectroscopy (XPS). Prior to Pt deposition, the atomic structure of the near-surface regions of the Ni(1 1 0)–(3 × 1)-O and NiO(1 1 0) structures were studied using CAICISS, finding changes to the interlayer spacings due to the adsorption of oxygen. Deposition of Pt on the Ni(1 1 0)–(3 × 1)-O surface led to a random substitutional alloy in the near-surface region at Pt coverages both below and in excess of 1 ML. In contrast, when the surface was treated with 1800 L of atomic oxygen in order to form a NiO(1 1 0) surface, a thin Pt layer was formed upon room temperature Pt deposition. XPS and LEED data are presented throughout to support the CAICISS observations.

Keywords: Low energy ion scattering (LEIS); X-ray photoelectron spectroscopy (XPS); Low energy electron diffraction (LEED); Platinum, Nickel; Oxidation

1. Introduction

Platinum is one of the most important metals used in modern heterogeneous catalytic processes, applied in the oxidation of CO and the reduction of NO molecules in vehicle exhaust systems, as well as in the oxidation of NH_3 molecules to form nitric acid and the production of specialist silicones [1–3]. However, Pt is an expensive material and therefore, in recent times, much attention has been paid to the characterisation of thin Pt films on a number of different substrates [4–8].

The oxidation of the Ni(1 1 0) surface has been studied using many different techniques (Refs. [9–13] cover just a few examples). Short exposures to molecular oxygen yield several reconstructions at sub-monolayer coverages. Firstly, the (3 × 1)-O *added row* structure is formed, with O atoms occupying every third row in the ⟨1 0 0⟩ direction, as shown in Fig. 1, corresponding to an O coverage of 0.33 ML. The structure of the Ni(1 1 0)–(3 × 1)-O surface has been studied by van der Veen et al. using medium energy ion scattering (MEIS), with an expansion found in the outermost interlayer spacing of ~1% relative to the bulk Ni(1 1 0) interlayer spacing [14]. Increasing the O coverage to 0.50 ML results in the formation of a (2 × 1)-O overlayer, with O atoms in every second row in the ⟨1 0 0⟩ direction. At a coverage of 0.67 ML, the (3 × 1)-O *missing row* structure is formed, with two out of every three rows in the ⟨1 0 0⟩ direction occupied by O atoms. Increasing the O coverage further results in the formation of a '*sub-oxide*' (9 × 5)-O structure at a coverage of a few ML, before a nickel oxide structure is formed at higher coverages [9].

Previous work on the characterisation of Pt deposition and O adsorption on Ni surfaces has been largely limited to attempts to oxidise the Ni substrate following Pt deposition. Such investigations on Ni(1 1 1) [15,16] and Ni(1 0 0) [17] have found that Pt growth proceeds in a

* Corresponding author. Tel.: +44 24 7652 4236.
E-mail address: c.f.mcconville@warwick.ac.uk (C.F. McConville).
[1] Present address: GlaxoSmithKline, St. George's Avenue, Weybridge, Surrey KT13 ODE, United Kingdom.
[2] Present address: Institut für Experimentalphysik, Johannes Kepler Universität Linz, Altenbergerstrasse 69, 4040 Linz, Austria.

0039-6028/$ - see front matter © 2006 Elsevier B.V. All rights reserved.
doi:10.1016/j.susc.2006.06.034

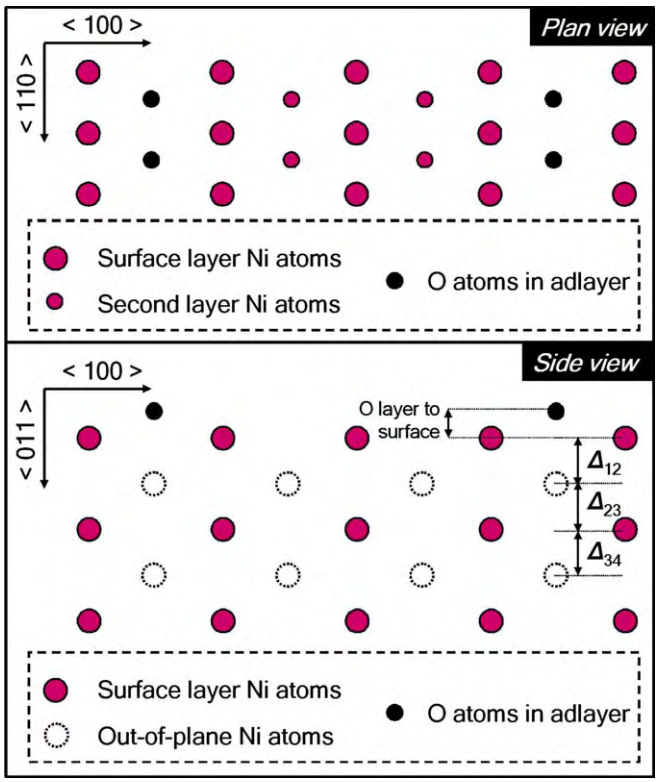

Fig. 1. A schematic illustration of the (3×1)-O added-row structure formed along rows in the $\langle 1\,0\,0\rangle$ direction on the Ni(1 1 0) surface. Both the top and side views of the structure are shown, with illustrations of the interlayer spacings, Δ_{ik}, and the spacing of the O adlayer and the Ni surface shown in the side view.

disordered fashion and that the Pt prevented the room temperature oxidation of the underlying Ni substrate. Kellogg showed that on the clean Ni(1 1 0) surface, Pt atoms replace Ni surface atoms to form a substitutional alloy at temperatures above 105 K [18], an observation confirmed by our recent study of this system [19]. In the work reported here, we aim to modify the growth mode of the Pt adlayer on the Ni(1 1 0) surface by exposing the surface to atomic oxygen prior to Pt deposition. This process may avoid alloying between the deposited Pt and the underlying Ni structure, producing a thin Pt film.

In this paper, we report the results of coaxial impact collision ion scattering (CAICISS) studies of the Ni(1 1 0)–(3×1)-O and NiO(1 1 0) surfaces, as well as differences in the growth characteristics of Pt upon these surfaces. CAICISS is a unique surface science technique which offers both compositional and structural information with a high degree of surface specificity. Recently this technique has been used for investigations of many adsorbate–substrate systems [4,20–26], and relies on the fact that the scattering of inert gas ions at relatively low energies (1–5 keV) from a surface can be described in terms of a simple binary collision model [26]. Analysis of the energy and flux of the scattered ions and neutral particles, as a function of incidence or azimuthal angle, offers the possibility to construct the atomic structure of the surface and determine the elemental composition with single-layer sensitivity. In addition, X-ray photoelectron spectroscopy (XPS) has been used to investigate the chemical state of the Ni and Pt atoms in the near-surface region, whilst low energy electron diffraction (LEED) has been used to verify the periodicity of the structures formed following the adsorption of oxygen on the Ni(1 1 0) surface.

2. Experimental details

The experiments were carried out in a UHV chamber equipped with a retractable 3-grid LEED optic (Omicron GmbH, Germany), a dual anode X-ray source (Vacuum Generators, UK), a 100 mm concentric hemispherical electron energy analyser (VSW, UK, HA100), and a modular CAICISS system described in detail elsewhere [4]. The main chamber is pumped by ion and diffusion pumps, and has a nominal base pressure in the region of 2×10^{-10} mbar. Resistive sample heating was monitored using a chromel–alumel thermocouple. XPS spectra were taken at a take-off angle of 45° using the Mg K_α anode of the X-ray source ($h\nu = 1253.6$ eV), with all binding energies calibrated relative to the Ni $2p_{3/2}$ peak at 852.3 eV [27].

2.1. Sample preparation

The Ni(1 1 0) crystal (Metal Crystals and Oxides, UK), cut to ±0.1° of the (1 1 0) plane (verified by Laue measurements), was spark eroded and mechanically polished prior to being mounted on to a manipulator capable of polar and azimuthal rotation. Once in the analysis chamber, the crystal was cleaned using cycles of low energy ion bombardment and annealing (IBA), with Ar^+ bombardment at 3 keV and extended annealing at 700 °C, until no impurities were observed in the XPS spectrum of the near-surface region and a sharp (1×1) LEED pattern was recorded. Atomic oxygen adsorption was performed using a thermal gas cracker (Oxford Applied Research, UK), consisting of a W tube heated via electron bombardment and surrounded by a water-cooled casing. The cracker had an estimated oxygen cracking efficiency of ~60% and was positioned with a direct line-of-sight to the Ni crystal surface. Pt deposition was achieved using a metal evaporation source consisting of a high purity Pt wire wound around a tungsten filament, with a current of 14.5 A passing through the filament. Previous experiments forming Pt overlayers on the Cu(1 0 0) surface were used to calibrate the deposition rate of the Pt source [28]. Pt deposition was carried out at pressures less than 1×10^{-8} mbar. The W 4d, C 1s and O 1s photoemission peaks were monitored to ensure that the surfaces were free from contamination both prior to and following Pt and O adsorption.

2.2. CAICISS setup

The modular CAICISS instrument used for this investigation is described in detail elsewhere [4]. All of the data presented in this paper were collected using a 3 keV He^+

ion beam produced from research grade helium. Data acquisition was carried out using an EG&G Ortec multichannel buffer (MCB) and Maestro II software. The polar angle data acquisition mode (polar scan) has been automated using a stepper motor, allowing data to be collected in 1.8° steps. For this investigation, an acquisition time of 100 s at each step was employed. All of the CAICISS data presented in this paper were collected in the ⟨1 0 0⟩ azimuth, as shown in Fig. 1. In this azimuth, the atomic structure is symmetric about the surface normal and therefore the 0–90° polar angle region is completely representative of the structure.

2.3. XPS and CAICISS data analysis

Structural information was obtained from CAICISS spectra by measuring the Ni and Pt-backscattered intensity as a function of polar angle after the preparation of each of the surfaces investigated. Due to its small differential scattering cross-section, oxygen atoms cannot be directly observed with the Warwick CAICISS system at the present time, and therefore the location of the O atoms has to be inferred from their effect on the Ni and Pt-backscattered intensity profiles. To enable accurate interpretation of the CAICISS data, the FAN simulation software developed by Niehus has been used to generate polar angle intensity plots from a range of 3D models in order to obtain the best fit for each experimental data set [29]. This package allows quantitative structural analysis, focussing on the relative intensities of the peaks within the spectrum and the angular position of the peaks relative to the experimental data. Many iterations were performed for each data set, changing the composition of layers in the surface region and corresponding interlayer spacings until an acceptable agreement with the experimental data was obtained. We have identified recently that care must also be taken over the choice of the ion–atom interaction potential for each element in the near-surface region [30]. Correction factors to the Firsov screening length in the Molière approximation to the Thomas–Fermi model (TFM) of 0.3 ± 0.1 for O, 0.60 ± 0.02 for Ni and 0.77 ± 0.02 for Pt were determined during the analysis of the data presented in this paper.

XPS data analysis was used to investigate the oxidation of the Ni surface, as well as to estimate the total amount of Pt deposited on the Ni(1 1 0)–(3 × 1)-O and NiO(1 1 0) surfaces. To estimate the Pt coverage, fitting involved the employment of a Gaussian–Lorentzian mixture (70%:30%) to determine the area of the Ni $2p_{3/2}$ peak prior to Pt deposition, as well as the Pt $4f_{7/2}$ and Ni $2p_{3/2}$ peaks following the deposition. Quantification methods outlined by Carley and Roberts [31] were then used to estimate the Pt surface concentration and total coverage, before a more accurate layer-by-layer Pt concentration profile was derived from the CAICISS data. A similar approach was taken to determine the total amount of O incorporated into the surface region during the oxidation process and to investigate the chemical environment of the Ni atoms in the surface region after the exposure of the Ni(1 1 0) crystal to atomic oxygen.

3. Results and discussion

3.1. The Ni(1 1 0)–(3 × 1)-O surface

Following the completion of the cleaning procedure outlined above, a (1 × 1) LEED pattern was recorded from the Ni(1 1 0) surface at 78 eV (Fig. 2(a)). The Ni(1 1 0)–(3 × 1)-O surface was formed by exposing the Ni(1 1 0) surface to 1.0 L of atomic oxygen at room temperature, with the (3 × 1) LEED pattern recorded at 92 eV shown in Fig. 2(b). CAICISS data were then recorded in the ⟨1 0 0⟩ azimuth, with the Ni-backscattered intensity profile extracted from the data shown in Fig. 3(a). In this profile, the peak at 14° corresponds to scattering from Ni atoms in the surface layer and represents an interatomic spacing (and also lattice constant) of 3.52 ± 0.05 Å, a value in line with the known lattice constant of Ni [32]. Moving to increasing polar angles, the peaks centered at 27°, 46°, 64° and 72° correspond to scattering from various scattering geometries in the sub-surface region, allowing the structure of the five outermost atomic layers to be derived.

Analysis of these data was carried out using the FAN software, with the simulated profile with the best fit shown in Fig. 3(b). The simulated profile arose from a structure with oxygen atoms located in sites directly above the second Ni layer atoms, with the O atoms occupying every third row in the ⟨1 0 0⟩ direction (as previously shown in Fig. 1). The O atoms were estimated to reside 1.0 ± 0.1 Å above the Ni(1 1 0) surface, the large error in their position due to the fact that as a result of its small differential scattering cross-section, O cannot currently be observed directly with the Warwick CAICISS system. However, locating the O atoms in this site led to an improved fit on the intensity of the surface peak at 14° when compared to the much reduced intensity given by other models,

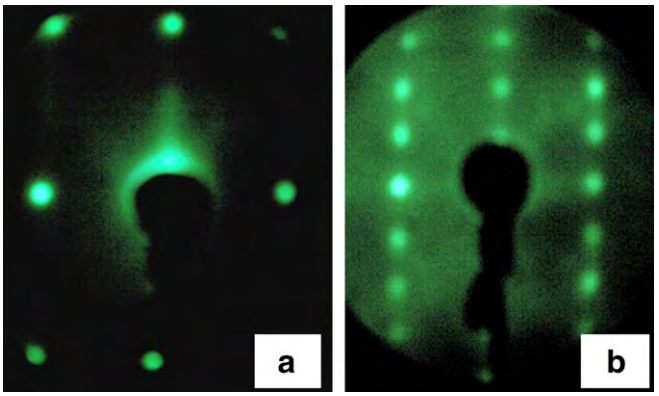

Fig. 2. LEED patterns observed from (a) the clean Ni(1 1 0) surface at 78 eV, and (b) the (3 × 1) pattern observed at 92 eV following exposure of the clean surface to 1.0 L of atomic oxygen.

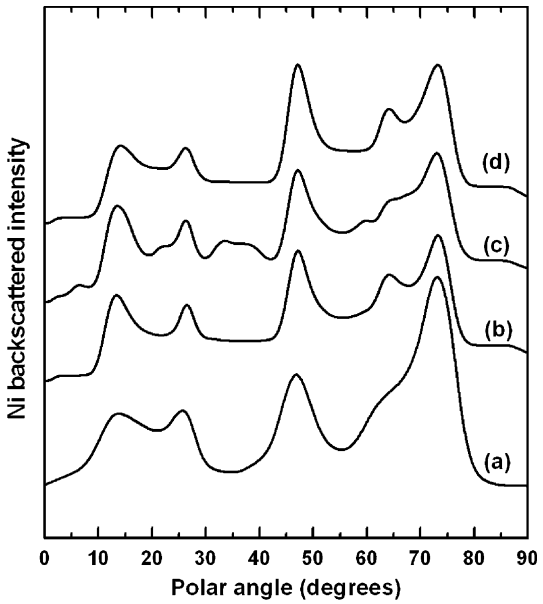

Fig. 3. (a) Experimental Ni-backscattered intensity profile from the Ni(1 1 0)–(3 × 1)-O surface in the ⟨1 0 0⟩ azimuth, showing peaks corresponding to scattering from the outermost five layers of the structure. (b) shows the corresponding profile from the FAN simulation of a trial structure containing expansions in the two outermost interlayer spacings relative to the bulk Ni(1 1 0) structure and O atoms in added rows running along the ⟨1 1 0⟩ direction. (c) and (d) show simulated profiles from models in which the added-rows consist of Ni–O chains in the ⟨1 1 0⟩ and ⟨1 0 0⟩ directions respectively. It should be noted that the experimental intensity at 72° is higher than any of the simulated profiles due to the existence of a small number of defects within the crystal structure.

including the 'missing row' (3 × 1)-O structure, in which every third row of O atoms is missing. Our model is also in contrast to the added-row structure reported by Eierdal and co-workers during their STM study of the adsorption of molecular oxygen on to the Ni(1 1 0) surface [9], in which the authors observed Ni–O chains on the surface. Fig. 3(c) and (d) shows that the inclusion of such chains into the structure leads to features which were not observed in the experimental CAICISS data. The structure derived from our CAICISS data contained a ~7% expansion of Δ_{12} (the spacing between the two outermost Ni layers), to 1.33 ± 0.02 Å. The expansion is larger than the 1% relaxation found by van der Veen et al. during their MEIS investigation of the Ni(1 1 0)–(3 × 1)-O surface [14]. The relaxation of the surface layer is also in contrast to published relaxation data from the clean Ni(1 1 0) surface which indicate a contraction of ~9% in Δ_{12} [33,34]. Such differences in the added-row structure and relaxations in the near-surface region are most likely due to the use of atomic oxygen in the current investigation. Δ_{23} was found to be 1.30 ± 0.02 Å, an expansion of ~4% on the bulk value and close to the value obtained from previous studies of the clean Ni(1 1 0) surface [33,34,36,37]. Below this, the bulk Ni(1 1 0) structure was observed, with interlayer spacings of 1.25 Å. Therefore, the adsorption of just 1/3 ML of oxygen was found to cause a significant outward relaxation of the surface layer, whilst the structure of the near-surface region (layers 2–5) was found to be unaffected.

3.2. Pt deposition on the Ni(1 1 0)–(3 × 1)-O surface

Following the deposition of 0.30 ± 0.03 ML of Pt on the Ni(1 1 0)–(3 × 1)-O surface at room temperature, no LEED pattern was observed, indicative of disorder in the surface region. The Pt spectrum extracted from the CAICISS data collected in the ⟨1 0 0⟩ azimuth is shown in Fig. 4(a). A brief inspection of this profile shows the existence of features centered at 25°, 47° and 72° arising from the scattering of particles from Pt atoms in the third atomic layer of the structure. This immediately indicates the penetration of Pt atoms into the near-surface region following sub-monolayer deposition at room temperature, whilst the surface peak, centered at 14°, shows a significant amount of Pt in the outermost layer.

Careful analysis of the CAICISS data using the FAN software yielded the Pt-backscattered profile shown in Fig. 4(b). In order to replicate the experimental profile, a surface layer with an average Ni_3Pt composition was required, in addition to Pt atoms making up 5% of the second and third atomic layers. The Pt atoms were located at random substitutional sites within the Ni(1 1 0) structure in accordance with the disorder indicated by the LEED observations. Interestingly, the analysis of the CAICISS data revealed no discernable change in the atomic structure of the surface region as a result of the inclusion of the Pt atoms, with Δ_{12} remaining at 1.33 ± 0.02 Å and Δ_{23} remaining at 1.30 ± 0.02 Å. The lack of change in the interlayer spacings is most likely due to the expansion of the outermost layers during the adsorption of O atoms prior to Pt deposition, making it easier for Pt atoms to be in-

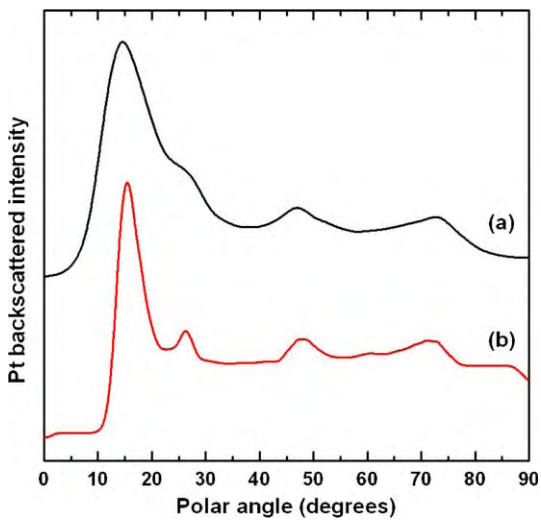

Fig. 4. (a) The Pt-backscattered intensity profile extracted from the CAICISS data collected in the ⟨1 0 0⟩ azimuth following the deposition of 0.30 ML of Pt on the Ni(1 1 0)–(3 × 1)-O surface. (b) The simulated Pt profile giving the best fit of this data. The final structure and compositional profile is summarized in Table 1.

cluded in the Ni(1 1 0) lattice without further disturbing the structure in a significant manner. The O atoms were observed to remain at a height of 1.0 ± 0.1 Å above the Ni–Pt surface alloy. No changes were observed in either the structure or composition of the sample at the fourth layer or below, which retained the bulk Ni(1 1 0) structure.

With evidence of a substitutional alloy at sub-monolayer Pt coverage, Pt deposition continued up to a total coverage in excess of a monolayer. CAICISS data were taken at coverages of 0.88 ± 0.05 ML and 1.88 ± 0.05 ML, with the Pt-backscattered intensity profiles extracted from the data taken in the ⟨1 0 0⟩ azimuth shown in Fig. 5 and the results of the compositional and structural analysis shown in Table 1. No LEED pattern was observed at either coverage, indicating that deposition of Pt on the Ni(1 1 0)–(3 × 1)-O surface at room temperature yields structures with little order at the surface in terms of the positioning of the Pt atoms within the Ni(1 1 0) structure.

The Pt-backscattered profiles shown in Fig. 5(b) (0.88 ML) and (c) (1.88 ML) show the increasing concentration of Pt atoms in the near-surface region, as evidenced by the increase in intensity of the peaks at polar angles in excess of 20°. Analysis of the profile collected following the deposition of 0.88 ML of Pt using the FAN software revealed the penetration of Pt atoms as far as the fourth atomic layer. It was also possible to conclude that Pt atoms make up $33 \pm 3\%$ of the surface layer, $25 \pm 2\%$ of the second layer and $15 \pm 2\%$ of both the third and fourth atomic layers.

Due to the 11.3% lattice mis-match between Ni and Pt, the inclusion of a significant number of the larger Pt atoms into the Ni(1 1 0) structure can be expected to produce expansions of the interlayer spacings in the near-surface region. This trend is shown by the shift in polar angle (~2°)

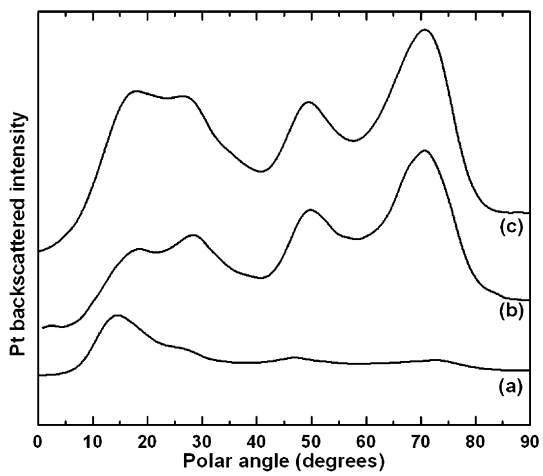

Fig. 5. The Pt-backscattered profiles extracted from the CAICISS data obtained at Pt coverages of (a) 0.30 ML, (b) 0.88 ML and (c) 1.88 ML on the Ni(1 1 0)–(3 × 1)-O surface. The surface peak is observed in the 14–16° region in all cases, whilst peaks arising from scattering in the near-surface layers (layers 2–5) are observed at higher polar angles. Structural and compositional details are given in the main text and Table 1.

Table 1
A summary of changes to the interlayer spacings and layer-by-layer concentrations during the deposition of Pt on the Ni(1 1 0)–(3 × 1)-O surface

Pt coverage (ML)	0.00	0.30	0.88	1.88
Surface layer Pt%	–	25	33	60
Layer 2 Pt%	–	5	25	55
Layer 3 Pt%	–	5	15	35
Layer 4 Pt%	–	0	15	20
Layer 5 Pt%	–	0	0	18
O layer to surface (Å)	1.0	1.0	1.2	1.3
Δ_{12}	+6.7%	+6.7%	+12.4%	+12.4%
Δ_{23}	+4.3%	+4.3%	+12.4%	+12.4%
Δ_{34}	0	0	+4.3%	+4.3%
Δ_{45}	0	0	0	0

for the peaks which correspond to scattering from subsurface Pt atoms as the coverage increases from 0.30 ML to 0.88 ML. Analysis of the intensity profile shown in Fig. 5(b) using the FAN software showed that Δ_{12} and Δ_{23} had both increased to 1.40 ± 0.02 Å, an expansion of ~12% on the bulk Ni(1 1 0) interlayer spacing, whilst Δ_{34} had expanded to 1.30 ± 0.02 Å, an expansion of ~4%. In order to accurately fit the shapes of the peaks observed, the (3 × 1)-O layer had to be moved to a height of 1.20 ± 0.05 Å above the surface layer of the alloy structure, again most probably due to the inclusion of the larger Pt atoms in the surface region.

The next Pt deposition stage, up to a total coverage of 1.88 ML, led to the inclusion of most of the newly deposited Pt into the two outermost layers of the crystal. The Pt concentration in the surface layer was observed to have increased to $60 \pm 3\%$, whilst the second layer Pt concentration increased to $55 \pm 3\%$. This is evidenced by the increase of the intensity of the surface peak at 16° in Fig. 5(c) relative to the other peaks in the Pt-backscattered profile, when compared to the profile obtained at a Pt coverage of 0.88 ML. The remaining newly deposited Pt was found to have migrated to the near-surface region, increasing the Pt concentration to $35 \pm 2\%$ in the third layer, $20 \pm 2\%$ in the fourth layer and $18 \pm 2\%$ in the fifth layer. However, the only change observed in the interlayer spacings was a movement of the (3 × 1)-O layer out to a height of 1.30 ± 0.05 Å above the surface.

3.3. The oxidised Ni(1 1 0) surface

3.3.1. LEED observations

The clean Ni(1 1 0)–(1 × 1) surface (Fig. 6(a)) was exposed to a series of short molecular O_2 doses, beginning with a 1.0 L exposure which yielded the (3 × 1)-O added-row structure (Fig. 6(b)). A total exposure of 1.5 L led to the (2 × 1)-O layer being formed on the surface (Fig. 6(c)), previously shown to correspond to an oxygen coverage of 0.5 ML [11,38]. A total exposure of 3.0 L led to the formation of the (3 × 1)-O missing row structure (Fig. 6(d)), corresponding to a 0.67 ML oxygen coverage.

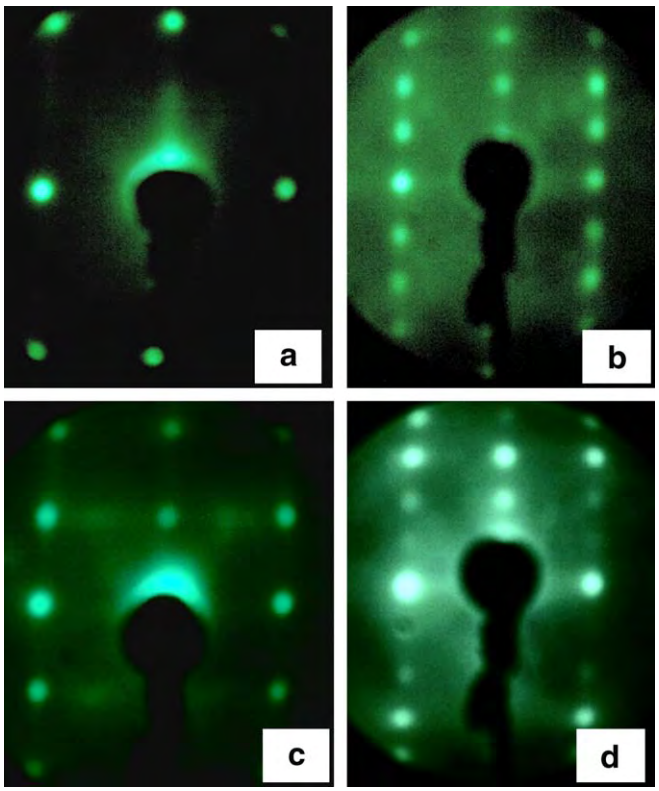

Fig. 6. (a) The (1 × 1) LEED pattern recorded from the clean Ni(1 1 0) surface, along with (b) the (3 × 1)-O added row following an oxygen exposure of 1.0 L, (c) the (2 × 1)-O structure observed following exposure of 1.5 L and (d) the (3 × 1)-O missing row structure observed following a total exposure of 3.0 L. The clean surface LEED pattern was recorded at 78 eV, whilst the remaining patterns were recorded at 92 eV.

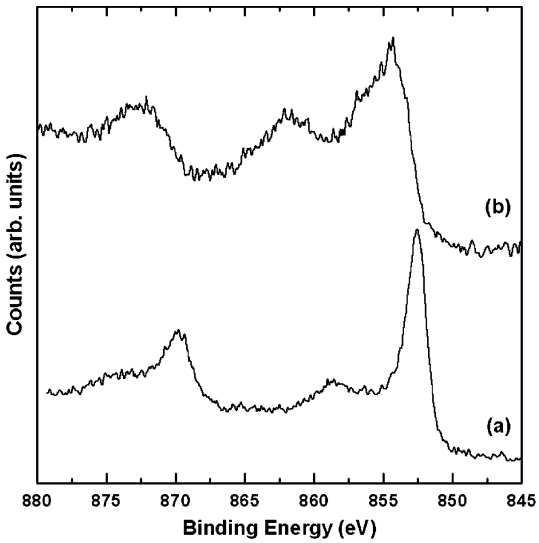

Fig. 7. The Ni 2p regions recorded from (a) the clean Ni(1 1 0) surface and (b) following exposure of the surface to 1800 L of atomic oxygen. Significant chemical shifts and no metallic Ni contributions were observed after oxygen exposure, indicating the formation of a thick NiO film. Indeed, (b) is identical to the spectrum generated from a NiO surface presented by Chastain [27].

Table 2
A summary of the Ni 2p and O 1s binding energies recorded before and after the exposure of the Ni(1 1 0) surface to 1800 L of atomic oxygen

XPS peak	Ni $2p_{1/2}$, eV	Ni $2p_{3/2}$, eV	O 1s, eV
Clean Ni(1 1 0) surface	852.3	869.8	n/a
NiO(1 1 0) surface	854.4	872.6	529.8
Energy shift	+2.1	+2.8	n/a

Further exposure, carried out using atomic oxygen to increase the efficiency of oxidation, led to the increase in the background intensity, obscuring any LEED spots. The (9 × 5) pattern reported previously was not observed in this investigation, most likely due to the use of atomic rather than molecular oxygen.

3.3.2. XPS measurements

The Ni 2p region of the XPS spectra collected following a total atomic oxygen exposure of 1800 L, along with the corresponding region collected from the clean Ni(1 1 0) surface are shown in Fig. 7. The clean surface Ni $2p_{1/2}$ and $2p_{3/2}$ peaks were observed at 852.3 and 869.8 eV respectively, along with the $2p_{3/2}$ satellite peak at 858.7 eV, and correspond well with previous data from clean Ni surfaces [27]. Chemical shifts of 1.9–2.8 eV, due to the incorporation of highly electronegative O atoms into the Ni structure, were seen in the Ni 2p peaks within XPS data collected following oxidation (see Table 2). Such a spectrum is typical of a nickel oxide surface [27]. No contribution from metallic Ni was observed, suggesting that a reasonably thick NiO film (in excess of 30 Å) had been formed on the Ni surface, given the 45° take-off angle employed during this investigation.

3.3.3. CAICISS investigations

Following the exposure of the Ni(1 1 0) surface to 1800 L of atomic oxygen, CAICISS data were taken in the ⟨1 0 0⟩ azimuth. The Ni-backscattered intensity profile is shown in Fig. 8. The first characteristic to note is that the peak positions arising from the NiO(1 1 0) surface throughout the polar angle range are very similar to those from the Ni(1 1 0)–(3 × 1)-O surface. This observation is in contrast with similar published experiments which have suggested the formation of a NiO(1 0 0) film on top of the Ni(1 1 0) substrate [9–11]. This is clearly not the case in our investigation, as a shift from a (1 1 0) surface to a (1 0 0) surface would produce large shifts in the peak positions observed in the CAICISS spectrum (as shown in Fig. 8(c)) due to the different scattering geometries within the fcc (1 0 0) and (1 1 0) structures [35]. Instead, the surface peak (at 14°) appears to have been reduced in intensity as a consequence of the disorder induced at the surface as a result of oxidation. This difference with previous investigations is again most likely due to the use of the more reactive atomic oxygen during the oxidation process as opposed to molecular oxygen.

Analysis of the Ni-backscattered profile using the FAN software revealed a ~6% expansion in both of the two out-

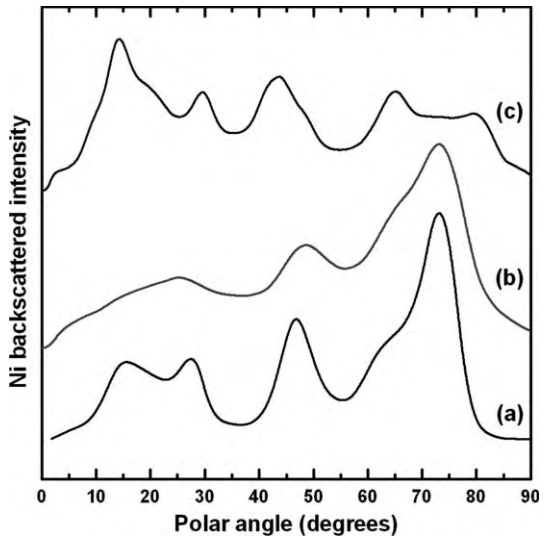

Fig. 8. The Ni-backscattered intensity profiles extracted from CAICISS data recorded from (a) Ni(1 1 0)–(3 × 1)-O surface and (b) the surface following exposure to 1800 L of atomic oxygen. Disorder at the surface is observed by the reduction of the intensity of the surface peak, but the overall structure remains largely unchanged during oxidation. A simulation of a NiO(1 0 0) surface (structure taken from the report by Muñoz-Márquez and co-workers [35]) is shown in (c), clearly demonstrating that such a surface has not been formed in this investigation.

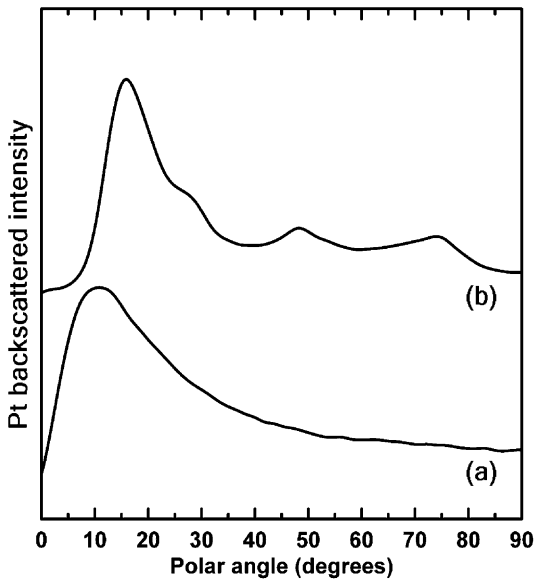

Fig. 9. (a) The Pt-backscattered intensity profile recorded with a 0.31 ML coverage of Pt on the NiO(1 1 0) surface. (b) The corresponding data following the deposition of 0.30 ML of Pt on the Ni(1 1 0)–(3 × 1)-O surface, clearly showing a shift in the surface peak and the existence of peaks at higher polar angles associated with the sub-surface Pt atoms.

ermost interlayer spacings, Δ_{12} and Δ_{23}. The bulk Ni(1 1 0) structure was observed deeper into the crystal, despite O atoms being found in substitutional sites throughout the probing depth of the CAICISS experiment (~5 layers). Whilst the formation of a thick NiO(1 1 0) film leaves the structure of the lattice near the surface practically unchanged when compared to the Ni(1 1 0)–(3 × 1)-O surface, the structure again represents a shift away from that of the clean Ni(1 1 0) surface [36,37].

3.4. Pt deposition on the NiO(1 1 0) film

Firstly, 0.31 ML of Pt was deposited on the NiO(1 1 0) film at room temperature. The Pt-backscattered intensity profile collected following the deposition is shown in Fig. 9(a). The profile does not exhibit any of the features at polar angles in excess of 25° which correspond to sub-surface Pt atoms, as observed following sub-monolayer Pt deposition on the Ni(1 1 0)–(3 × 1)-O surface (Fig. 9(b)). Therefore, virtually all of the Pt atoms must be located in the outermost layer (i.e., in a film on top of the surface). In this case, the surface peak in the Pt profile was observed to have shifted from 16° (Pt on the Ni(1 1 0)–(3 × 1)-O surface) to 10° (Pt on NiO(1 1 0)). This indicates a much larger average spacing between Pt atoms in the outermost layer, again a feature which indicates the formation of a Pt overlayer. The surface peak was also broadened in the Pt/NiO(1 1 0) case, indicating a range of spacings between Pt atoms on the surface which would only be possible if the Pt atoms were not contained within the NiO(1 1 0) film.

Further evidence for the formation of a thin Pt layer on top of the NiO(1 1 0) film comes from the XPS data recorded following the deposition of Pt on the surface. The data, presented in Fig. 10, shows a comparison of the Pt 4f regions recorded from a clean Pt(1 1 1) surface and an oxidised Pt(1 1 1) surface from a previous investigation

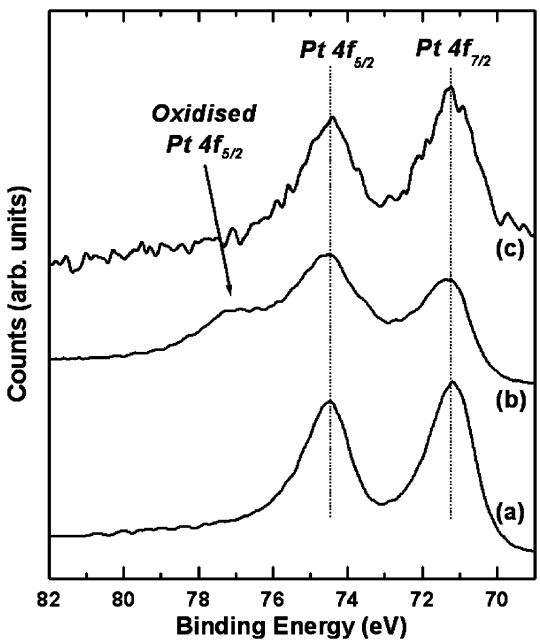

Fig. 10. The Pt 4f region recorded from three different samples. (a) The data recorded from a clean Pt(1 1 1) surface [4]. (b) The data collected following the oxidation of the Pt(1 1 1) surface, showing an additional feature at 76.8 eV [4]. (c) The Pt 4f region recorded following the deposition of 0.31 ML of Pt on the NiO(1 1 0) surface.

[4], with the data recorded from the Pt layer on top of the NiO(1 1 0) film. The data collected from both the clean Pt(1 1 1) surface and following Pt deposition on the NiO(1 1 0) film exhibit just two peaks in the Pt 4f region, corresponding to the peaks expected from a clean Pt surface [27]. Data recorded from the Pt 4f region following the oxidation of a Pt(1 1 1) surface exhibits an additional shoulder at 76.8 eV due to the formation of an oxide layer at the surface. This feature was absent in the Pt 4f region recorded following Pt deposition on the NiO(1 1 0) film, indicating that there was very little interaction between the Pt and O atoms within the sample and pointing to the formation of a Pt overlayer on top of the NiO(1 1 0) film.

A second Pt deposition was implemented, bringing the total Pt coverage to 0.80 ML, in order to provide further evidence for the formation of a Pt layer on the NiO(1 1 0) film. The Pt-backscattered intensity profile, shown in Fig. 11, again shows a very broad surface peak due to the range of spacings between the Pt atoms in the adlayer. However, no peaks of significant intensity are observed at higher polar angles – peaks which would be present if only a small amount of Pt atoms (~5% of a monolayer) had penetrated into the NiO(1 1 0) structure. In this case, there is only a slight suggestion of peaks at ~40°, 54° and 78°, most likely due to the start of the formation of a second layer of Pt in small regions on the surface. The Pt surface peak was found to be centered at 17°, a 5° shift to higher angles compared to the data recorded following the 0.31 ML Pt deposition on the NiO(1 1 0) film. This shift should be expected as it arises from the shortening of the average spacing between Pt atoms in the ⟨1 0 0⟩ direction

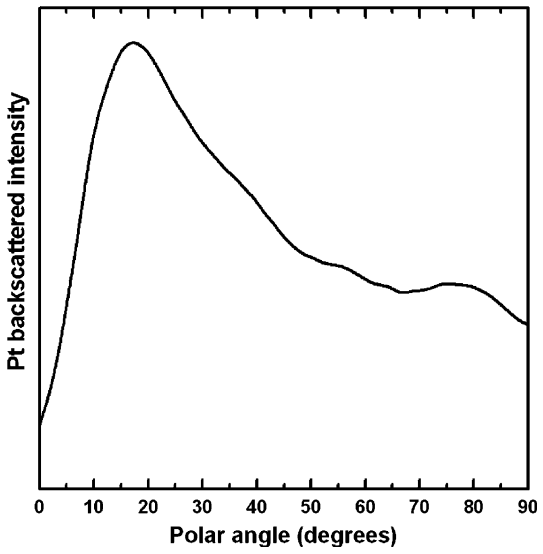

Fig. 11. The Pt-backscattered intensity profile recorded in the ⟨1 0 0⟩ azimuth following the deposition of 0.80 ML of Pt on the NiO(1 1 0) surface at room temperature. The broad surface peaks arises from the range of distances between Pt atoms in the adlayer, whilst the lack of peaks at polar angles in excess of ~30° suggests the layer-by-layer growth of a purely Pt film.

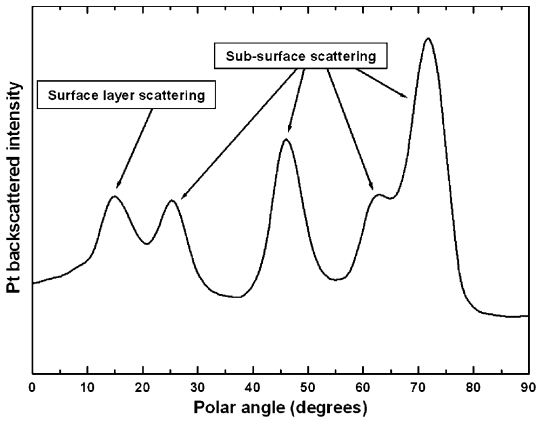

Fig. 12. The Pt-backscattered intensity profile recorded in the ⟨1 0 0⟩ azimuth following annealing of a sample containing a 0.80 ML Pt film on top of a NiO(1 1 0) surface to 400 °C for 10 min. The presence of the sharp peaks at polar angles in excess of ~20° indicates a well-ordered structure with a significant amount of Pt atoms which have penetrated into the near-surface region during the annealing process.

which occurs as the Pt layer nears completion. These observations indicate that a purely Pt layer has been formed on top of the NiO(1 1 0) film.

Following the acquisition of CAICISS data at a Pt coverage of 0.80 ML, the sample was annealed to 400 °C for 10 min. A weak (1 × 1) LEED pattern was observed on cooling to room temperature, indicating that the surface region had undergone some re-ordering during the annealing. The Pt-backscattered intensity profile extracted from the CAICISS data recorded from this surface is shown in Fig. 12. The surface peak, at 15°, corresponds well with the angle of the surface peak observed following Pt deposition on the Ni(1 1 0)–(3 × 1)-O surface (16°, as shown in Fig. 5). Therefore, it appears that the Pt atoms are now located within the Ni(1 1 0) lattice. The peaks centered at 25°, 47°, 63° and 72° all indicate that the Pt atoms have penetrated well below the surface, to at least the fifth layer of the structure. In addition, the annealing appears to have removed a significant proportion of the O atoms and disorder from the surface region, as evidenced by the sharpness of all the peaks in the CAICISS profile. This demonstrates that sub-surface Pt atoms can be clearly observed using CAICISS and that before annealing, the Pt atoms were residing in a purely Pt layer on top of the NiO(1 1 0) film.

4. Conclusions

The deposition of Pt on the clean Ni(1 1 0) surface has previously been shown to produce a substitutional alloy at the surface [18]. In this paper, the effect on the growth of Pt on Ni(1 1 0) surfaces by pre-exposing the Ni crystal to varying amounts of atomic oxygen has been investigated using CAICISS, LEED and XPS.

The surface was firstly exposed to 1.0 L of atomic oxygen, after which LEED indicated that the Ni(1 1 0)–(3 × 1)-O surface had been formed. Analysis of CAICISS

data recorded in the ⟨1 0 0⟩ azimuth led to the conclusion that this corresponded to the (3 × 1)-O added-row structure, as opposed to the (3 × 1)-O missing row structure, with the added rows consisting of only O atoms along the ⟨1 1 0⟩ direction. The CAICISS data also illustrated the relaxations induced in the surface region as a result of the adsorption of just 1/3 ML of atomic oxygen, with the outermost interlayer spacing, Δ_{12}, found to have expanded by ~7% with respect to the bulk Ni(1 1 0) structure. Δ_{23} was also observed to have expanded to ~4% more than the bulk interlayer spacing, although this is in line with previous investigations of the structure of the clean Ni(1 1 0) surface.

The deposition of 0.30 ML of Pt on the Ni(1 1 0)–(3 × 1)-O surface led to the formation of a Ni–Pt alloy in the surface region. Pt atoms were observed to have penetrated as far as the third layer of the structure, although no changes to the near-surface structure were observed. However, a further Pt deposition which brought the total coverage to 0.88 ML resulted in the first two interlayer spacings expanding to ~12% larger than the bulk Ni(1 1 0) interlayer spacing, along with a ~4% expansion of Δ_{34} due to the inclusion of Pt atoms in the fourth atomic layer. Increasing the deposited Pt coverage to 1.88 ML led to an increase in the Pt concentration in each of the outermost five layers of the structure, but produced no discernable change in the interlayer spacings in the near-surface region. The (3 × 1)-O layer was observed to remain on top of the Ni–Pt surface alloy throughout the investigation.

Following the re-preparation of a clean Ni(1 1 0) surface, the sample was exposed to a series of short molecular O_2 exposures which allowed the (3 × 1)-O missing row, (2 × 1)-O and (3 × 1)-O added-row structures to be observed with LEED. All LEED spots were concealed by the increasing background intensity as the surface was exposed to further amounts of atomic oxygen.

After an extended exposure to atomic oxygen (1800 L), XPS showed that a NiO film of at least 30 Å in thickness had been formed on the surface, with no purely metallic Ni observed within the sampling depth. CAICISS indicated that a NiO(1 1 0) film had been produced during the oxygen exposure, contrary to some previous reports which have suggested that this film should take on a NiO(1 0 0) structure. This fundamental difference was most likely due to the use of atomic oxygen during this investigation.

Pt was deposited up to a total coverage of 0.80 ML on the NiO(1 1 0) film at room temperature. CAICISS and XPS observations suggested that all of the Pt atoms were located on top of the NiO(1 1 0) structure in a disordered, but purely Pt layer, and hence the initial growth of Pt deposited at room temperature was found to be different when compared to the clean Ni(1 1 0) and Ni(1 1 0)–(3 × 1)-O surfaces. This opens the possibility of the formation of Pt thin films on NiO(1 1 0) for application in fuel cells, the production of specialist silicones, the formation of nitric acid and other modern industries. Annealing of the Pt/NiO(1 1 0) structure led to the formation of a Ni–Pt alloy in the near-surface region and hence to the elimination of the Ni-oxide structure.

Acknowledgements

Rob Johnston is thanked for technical support during this investigation. M. Walker and M.G. Brown thank the EPSRC for Graduate Studentships from the Doctoral Training Account. M. Draxler acknowledges the support of the Austrian Science Fund (FWF) via an Erwin Schrödinger Fellowship (Project Number J2417-N08).

References

[1] A. Eichler, J. Hafner, Surf. Sci. 433–435 (1999) 58.
[2] W.D. Mieher, W. Ho, Surf. Sci. 322 (1995) 151.
[3] M.A. Brook, Biomaterials 27 (2006) 3274.
[4] C.R. Parkinson, M. Walker, C.F. McConville, Surf. Sci. 545 (2003) 19.
[5] C.P. Oliver, B.V. King, D.J. O'Connor, Surf. Sci. 557 (2004) 101.
[6] C. Egawa, S. Endo, H. Iwai, S. Oki, Surf. Sci. 474 (2001) 14.
[7] G.F. Cabeza, P. Légaré, A. Sadki, N.J. Castellani, Surf. Sci. 457 (2000) 121.
[8] D.K. Flynn, J.W. Evans, P.A. Thiel, J. Vac. Sci. Technol. A 7 (1989) 2162.
[9] L. Eierdal, F. Besenbacher, E. Lzegsgaard, I. Stensgaard, Surf. Sci. 312 (1994) 31.
[10] R.G. Smeenk, R.M. Tromp, J.F. van der Veen, F.W. Saris, Surf. Sci. 95 (1980) 156.
[11] K. Yagi-Watanabe, Y. Ikeda, Y. Ishii, T. Inokuchi, H. Fukutani, Surf. Sci. 482–485 (2001) 128.
[12] R.L. Park, H.E. Farnsworth, J. Appl. Phys. 35 (1964) 2220.
[13] K. Suzuki, A. Yamane, R. Ozawa, Y. Gunji, K. Higashiyama, H. Fukutani, Surf. Sci. 365 (1996) 248.
[14] J.F. van der Veen, R.G. Smeenk, R.M. Tromp, F.W. Saris, Surf. Sci. 79 (1979) 212.
[15] S. Deckers, F.H.P.M. Habraken, W.F. van der Weg, J.W. Geus, Appl. Surf. Sci. 45 (1990) 207.
[16] S. Deckers, S. Offerhaus, F.H.P.M. Habraken, W.F. van der Weg, Surf. Sci. 237 (1990) 203.
[17] S. Deckers, F. Bisschop, D. de Jager, S.H. Offerhaus, J. van Roijen, F.H.P.M. Habraken, W.F. van der Weg, Surf. Sci. 258 (1991) 82.
[18] G.L. Kellogg, Phys. Rev. Lett. 67 (1991) 216.
[19] M. Walker, M. Draxler, C.R. Parkinson, C.F. McConville, Nucl. Instr. Meth. B 249 (2006) 314.
[20] T.C.Q. Noakes, D.A. Hutt, C.F. McConville, D.P. Woodruff, Surf. Sci. 372 (1997) 117.
[21] H. Niehus, M. Voetz, C. Achete, K. Morgenstern, G. Cosma, in: R.J. MacDonald, E. Taglauer, K. Wandelt (Eds.), Surface Science, Principles and Current Applications, Springer, 1996, p. 38.
[22] Y. Saito, Y. Tanabe, T. Yamaguchi, N. Teraguchi, A. Suzuki, T. Araki, Y. Nanishi, Phys. Stat. Sol. (b) 228 (2001) 13.
[23] K. Xu, A. Yoshikawa, Appl. Phys. Lett. 83 (2003) 251.
[24] T. Ohnishi, K. Takahashi, M. Nakamura, M. Kawasaki, M. Yoshimoto, H. Koinuma, Appl. Phys. Lett. 74 (1999) 2531.
[25] R. Tsushima, M. Katayama, T. Fujino, M. Shindo, T. Okuno, K. Oura, Appl. Surf. Sci. 216 (2003) 19.
[26] H. Niehus, W. Heiland, E. Taglauer, Surf. Sci. Rep. 17 (1993) 213.
[27] J. Chastain, R.C. King Jr. (Eds.), Handbook of X-ray Photoelectron Spectroscopy, Physical Electronics, Eden Prairie, 1995.
[28] M. Walker, C.R. Parkinson, M. Draxler, C.F. McConville, Surf. Sci. 584 (2005) 153.
[29] H. Niehus, FAN Simulation Software, Humboldt-Universität zu Berlin, Institut für Physik, Berlin. Available from: <http://asp2.physik.hu-berlin.de/>.

[30] M. Draxler, M. Walker, C.F. McConville, Nucl. Instr. Meth. B 249 (2006) 812.
[31] A.F. Carley, M.W. Robers, Proc. R. Soc. Lond. A 363 (1978) 403.
[32] S.M. Foiles, M.I. Baskes, M.S. Daw, Phys. Rev. B 33 (1986) 7983.
[33] S.M. Yalisove, W.R. Graham, E.D. Adams, M. Copel, T. Gustafsson, Surf. Sci. 171 (1986) 400.
[34] C. Xu, D.J. O'Connor, Nucl. Instr. Meth. B 42 (1989) 251.
[35] M.A. Muñoz-Márquez, R.E. Tanner, D.P. Woodruff, Surf. Sci. 565 (2004) 1.
[36] A.M. Rodríguez, G. Bozzolo, J. Ferrante, Surf. Sci. 289 (1993) 100.
[37] N. Ting, Y. Qingliang, Y. Yiying, Surf. Sci. 206 (1988) L857.
[38] P.R. Norton, P.E. Bindner, T.E. Jackman, Surf. Sci. 175 (1986) 313.